Behavior of Si Photoelectrodes under High Level Injection Conditions. 3. Transient and Steady-State Measurements of the Quasi-Fermi Levels at Si/CH_3OH Contacts

C. N. Kenyon, Ming X. Tan, Olaf Krüger, and Nathan S. Lewis*

Division of Chemistry and Chemical Engineering, California Institute of Technology, Pasadena, California 91125

Received: August 14, 1996; In Final Form: December 3, 1996[⊗]

Real-time measurements of the photovoltage rise and decay at the back of lightly doped, thin, long lifetime Si photoelectrodes were recorded subsequent to a variety of spatial and temporal carrier generation impulses. The functional form of the rising portion of the photovoltage signal is sensitive to charge transport processes, and this signal was used to validate experimentally the hypothesis that charge transport in these samples under high level injection is primarily driven by diffusion, as opposed to drift. The decay of the photovoltage signal back to its equilibrium value yielded information concerning the surface recombination velocity, S_f, of the various Si/CH_3OH redox couple contacts. These data validated the relatively high surface quality of the Si/liquid interface in contact with a variety of redox species. Furthermore, the low surface recombination velocities are in agreement with prior theoretical and experimental estimates of interfacial charge-transfer rate constants for semiconductors in contact with nonadsorbing, outer-sphere, redox species. The front surface recombination velocity data also provided a needed boundary condition for modeling the carrier concentration dynamics and allowed quantification of the difference between the quasi-Fermi levels at the back and front surfaces of the samples at all times of experimental interest. Digital simulation and analytical modeling were performed to compute the gradients in the quasi-Fermi levels for samples operated under steady-state, open-circuit, high level injection conditions. In no case was the difference between the quasi-Fermi level value at the back of the sample and its value at the solid/liquid contact greater than 10 meV. These data, combined with those described in parts 1 and 2, comprise a relatively complete picture of the transport and recombination processes that occur at these types of semiconductor/liquid contacts.

I. Introduction

The preceding papers described the use of a novel photoelectrode geometry to effect efficient carrier separation through diffusion-driven concentration gradients. In this electrode configuration, implanted n^+ and p^+ point contacts at the back of Si electrodes have allowed simultaneous measurements of the apparent electrochemical potentials (quasi-Fermi levels) for electrons and holes in a semiconductor photoelectrode. These measurements, performed under various steady-state illumination conditions, have yielded valuable insight into the behavior of the theoretically important quasi-Fermi level positions. Experimental data have been collected on the behavior of the electron ($\mathbf{E}_{F,n}$) and hole ($\mathbf{E}_{F,p}$) quasi-Fermi levels for four redox couples (with redox potentials spanning over 1 V), whose electrical junction characteristics ranged from rectifying to ohmic. These data were in excellent agreement with the predictions of theoretical models for the behavior of quasi-Fermi levels under steady-state conditions.[1,2]

One important quantitative issue involved in interpreting these experimental data is the degree to which, under high level injection conditions, the quasi-Fermi level positions measured at the back point contacts of the sample approximate the positions of the quasi-Fermi levels at the semiconductor/liquid interface. These latter values are the ones of direct theoretical interest and are those required to describe the interfacial charge carrier kinetics at solid/liquid contacts. Although to our knowledge no previous direct experimental data exist on the positions of the quasi-Fermi level values at semiconductor/liquid interfaces,[3] the desired quantities could, in principle, be determined through strategies that exploit near-surface conductance data.[4] However, the surface conductance approach would require fabrication of a rather complex lithographic structure (to measure both electron and hole concentrations simultaneously) and would introduce other contact and recombination regions into the device design that must be considered during a full analysis of the system.

An alternative approach, described herein, is to develop a functional model of the relevant kinetic processes for the semiconductor/liquid contact of interest. Knowledge of carrier transport, generation, and recombination in the photoelectrode would provide a description of the electron and hole concentration profiles ($n(x,t)$ and $p(x,t)$, respectively) as a function of time (t) and distance (x) from the solid/liquid contact. According to the definitions of the quasi-Fermi levels when Boltzmann-type statistics applies,[5] given in eqs 1 and 2, a complete spatial description of the carrier concentration profiles would allow explicit computation of the difference in quasi-Fermi level positions between the front ($x = 0$) and back ($x = d$) surfaces:

$$\mathbf{E}_{F,n}(0,t) - \mathbf{E}_{F,n}(d,t) = kT \ln\left[\frac{n(d,t)}{n(0,t)}\right] \quad (1)$$

$$\mathbf{E}_{F,p}(0,t) - \mathbf{E}_{F,p}(d,t) = kT \ln\left[\frac{p(0,t)}{p(d,t)}\right] \quad (2)$$

where k is the Boltzmann constant, T is the temperature, q is the elementary charge, and d is the sample thickness. The purpose of this work is to develop, and experimentally validate, a complete spatial and temporal model for the carrier concentrations of the photoelectrodes discussed in parts 1 and 2 of this series.[6,7]

Several approaches were pursued to achieve these goals. Real-time measurements of the photovoltage rise and decay at the back of the sample were performed in response to a variety of spatial and temporal carrier generation impulses (Figure 1).

* To whom correspondence should be addressed.

⊗ Abstract published in *Advance ACS Abstracts,* February 1, 1997.

S1089-5647(96)02485-6 CCC: $14.00 © 1997 American Chemical Society

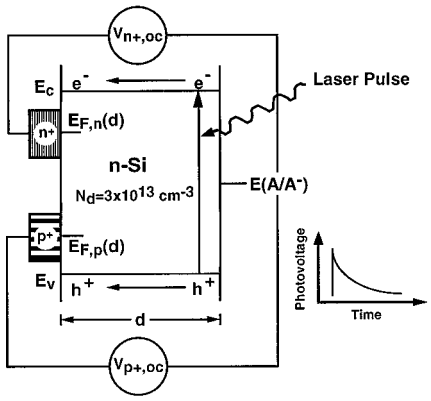

Figure 1. A schematic representation of the real-time photovoltage rise and decay measurements at a high purity Si/liquid junction. $\mathbf{E}_c$ and $\mathbf{E}_v$ represent the conduction band edge and valence band edge of the semiconductor, respectively. $\mathbf{E}(A/A^-)$ is the solution electrochemical potential. The wavelength of the laser pulse can be adjusted to provide the desired carrier generation profiles in the semiconductor. The photovoltages measured at the n^+ and p^+ contact points directly reflect the quasi-Fermi level positions of electrons and holes at the back of the sample, $\mathbf{E}_{F,n}(d) = qV_{n+,oc}$ and $\mathbf{E}_{F,p}(d) = qV_{p+,oc}$. The rise and decay of the quasi-Fermi levels are functions of the carrier transport, generation, and recombination processes of the system.

The functional form of the rising portion of the photovoltage signal is sensitive to charge transport processes,[8,9] and this signal was therefore used to validate experimentally the hypothesis that charge transport in these samples under high level injection is primarily driven by diffusion, as opposed to drift. The decay of the photovoltage signal back to its equilibrium value yielded additional information concerning the surface recombination velocity, S_f, of the various Si/CH_3OH contacts. These data provided a needed boundary condition for modeling the carrier concentration dynamics and allowed quantification of the difference between the quasi-Fermi levels at the back and front surfaces of the samples at all times of experimental interest. Digital simulation and analytical modeling have also been performed to compute the gradients in the quasi-Fermi levels for samples operated under steady-state, open-circuit, high level injection conditions. This analysis did not require any information from the transient experiments or modeling thereof, but served to validate further the values determined from the transient experiments, and lent confidence to the overall description of the carrier dynamics in this system.

II. Experimental Section

The procedures for sample preparation were identical to those described in part 1,[6] as were the procedures for redox couple, electrolyte, and solvent preparation and purification. Electrochemical instrumentation was also identical with that described in part 1, except for the instrumentation used in recording the transient photovoltage signals. These procedures, and information germane to the accompanying simulation and modeling methods, are described below.

Transient photovoltage measurements were performed using three channels of a Tektronix 11A34 amplifier (300 MHz bandwidth) in a Tektronix DSA600 digital oscilloscope. Channels 1 and 2 were connected to the p^+ and n^+ point contacts, respectively. A Pt wire immersed in the solution served as the reference electrode, and channel 3 was connected to this wire. The point contacts on the Si were effectively maintained at open circuit from the other contacts by imposing 1 MΩ input impedances onto channels 1 and 2, with the reference Pt wire grounded by selecting a 50 Ω input impedance for channel 3. Signals were simultaneously acquired from all three channels. The data were collected and converted into one signal, representing [(channel 1 − channel 3) − (channel 2 − channel 3)], before signal averaging. The averaged signal was then transferred through a GPIB interface to a PC for storage and subsequent analysis.

Illumination was provided by a Quanta-Ray Model DCR Nd:YAG laser, which had a pulse width of approximately 10 ns fwhm for both the fundamental (1064 nm) and frequency-doubled (532 nm) outputs. The laser beam was expanded to illuminate the entire electrode area (≈1.1 cm^2), and the beam intensity was varied using either the Q-switch delay control and/or neutral density filters. Approximate beam powers were measured using a joule meter that had been masked to expose an area equal to that of the electrode.

The BASIC program used in the digital simulation was a modified version of a finite-difference program originally written by N. S. Lewis. The unmodified program has been described in detail by Ryba,[10] and both the original and modified versions are available on request. Carrier concentrations as a function of time and distance were computed and stored in separate data files. A DOS-compatible Macintosh Quadra 610 was used to run the simulations.

III. Results

A. Time-Resolved Photovoltage Studies: Measurement and Simulation of the Time-Dependent Carrier Concentration Profiles at Si/$CH_3OH-Me_2Fc^{+/0}$ Contacts. *1. Time-Resolved Photovoltage and Carrier Concentration Data.* Figure 2a,b depicts the transient photovoltage signals that were observed after injection of charge into a Si photoelectrode in contact with $CH_3OH-Me_2Fc^{+/0}$. In these figures, the difference in photovoltage measured between the p^+ and n^+ contact points relative to the solution potential ($V_{p+,oc}$ and $V_{n+,oc}$, respectively) has been plotted against time. Data were only analyzed for $V_{p+,oc} - V_{n+,oc} \geq 450$ mV, to ensure that the analyzed data were obtained when the back of the sample was in high level injection. Figure 3 displays similar photovoltage data, except that the carrier injection was performed with light of wavelength 1064 nm instead of with 532 nm illumination.

According to the definitions of quasi-Fermi levels,[5] the value of $V_{p+,oc}(t) - V_{n+,oc}(t)$ is related to the product of the electron and hole concentrations at the back surface of the sample ($n(d,t)$ and $p(d,t)$, respectively) through eq 3:[11]

$$n(d,t)\,p(d,t) = n_i^2 \exp\left[\frac{qV_{p+,oc}(t) - qV_{n+,oc}(t)}{kT}\right] \qquad (3)$$

In this equation, n_i is the intrinsic carrier concentration, and the Boltzmann-type relationship of this equation holds as long as neither quasi-Fermi level is within ≈3kT of a band edge energy.

For an initial donor density N_d and with initial injected carrier concentrations $\Delta n(x,0)$ and $\Delta p(x,0)$, the inequalities $\Delta n(x,t) \gg N_d$ and $\Delta p(x,t) \gg n_i^2/N_d$ must be satisfied when the sample is under high level injection conditions. Under these conditions, $n(d,t) \cong p(d,t)$. Use of this approximation in eq 3 yields the following relationship between the measured voltage, $V_{p+,oc}(t) - V_{n+,oc}(t)$, and the carrier concentrations:

$$n(d,t) = p(d,t) = n_i \exp\left[\frac{qV_{p+,oc}(t) - qV_{n+,oc}(t)}{2kT}\right] \qquad (4)$$

Using eq 4, the transient photovoltage data of Figure 2a,b were readily converted into the desired time-dependent carrier concentrations at the back of the sample. For the experiment of Figure 2a,b, the carrier concentration data have been displayed as Figure 2c,d.

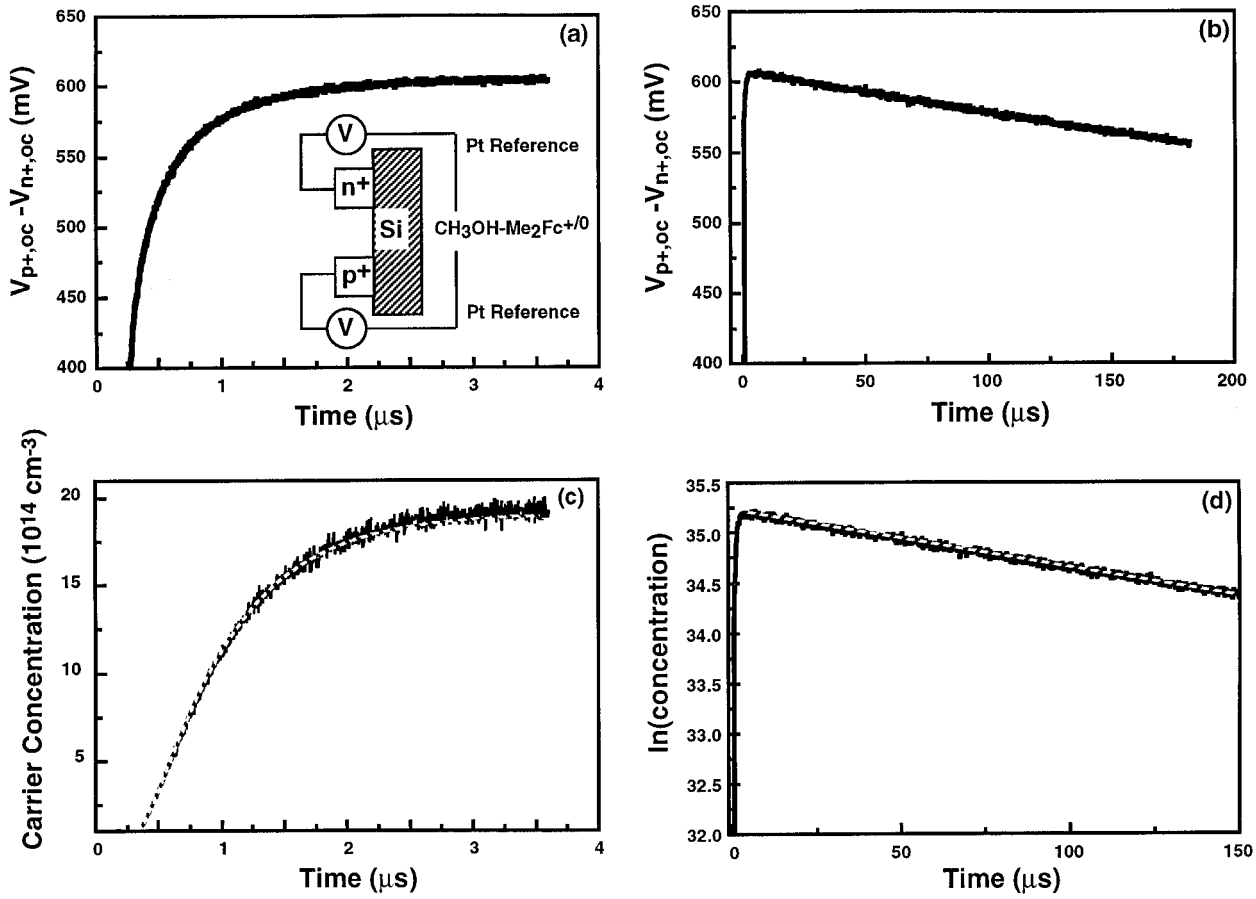

Figure 2. Photovoltage ($V_{p+,oc} - V_{n+,oc}$) rise (a) and decay (b) measured at the Si/CH_3OH−1.0 M $LiClO_4$−3.9 mM Me_2Fc−0.6 mM Me_2FcBF_4 contact under 532 nm pulsed laser illumination (≈2 × 10^{-5} J cm^{-2}). The solid line in (c) represents the rise signal of the carrier concentration at the back of the sample calculated from the $V_{p+,oc} - V_{n+,oc}$, values presented in (a) using eq 4. The dashed line is the fit generated from the diffusional model of eqs 7−11. The thickness of the sample, d, obtained from the fit was 107 μm. The value of I_0' was 2.05 × 10^{13} cm^{-2}. In (d), a semilog plot of the carrier concentration vs time is presented (solid line). The dashed line represents the linear fit to the decay portion of the concentration profile. The slope of this line corresponded to a surface recombination velocity of 60 cm s^{-1} (eq 6).

2. Semiquantitative Analysis of Carrier Decay Dynamics. The functional form of the concentration rise data contained information on the carrier transport dynamics, while the time constant for decay of the carrier concentration allowed calculation of the surface recombination velocity, S_f. In this section, we discuss approximate solutions that have yielded significant physical insight into the photovoltage rise and decay signals. We then proceed in section III.A.3 to describe the results of a complete digital simulation of the carrier decay dynamics.

As shown in Figure 2c, the carrier concentration reached an approximately constant value after 3 μs, demonstrating that recombination occurred at a much slower rate than carrier diffusion. Under such conditions, for $t > 2$ μs the carrier concentrations $p(x,t)$ and $n(x,t)$ are essentially independent of distance. As described below, this difference between the experimental time scales for transport and recombination in the sample facilitates the use of approximate analytical solutions to describe the photovoltage signals in each separate time regime. We will first discuss the photovoltage decay dynamics and will then proceed to analyze the form of the rising portion of the photovoltage signal.

When the carrier concentration is essentially independent of position in the sample, the carrier concentration decay dynamics can be readily related to the surface recombination velocity (S_f), provided that the decays result predominantly from recombination at the solid/liquid interface. Because the bulk lifetime of these samples was >1 ms[12] and because the photovoltage decay time constant for these same structures exceeded 250 μs in air (when the front surface of the sample was protected with a passivation layer to minimize surface recombination), all decays observed for semiconductor/liquid junctions (after removal of the front surface passivation layer with a chemical etch) with a decay time < 250 μs, including those in Figures 2 and 3, were reliably ascribed to front surface recombination/charge transfer processes at the solid/liquid contact.

Under these conditions, reference to the behavior of the fundamental filament decay mode yields[13,14]

$$-\frac{dp(t)}{dt} = \frac{p(t)}{\tau_f} = p(t)\frac{S_f}{d} \tag{5}$$

$$\ln(p(t)) = \ln(p_0) - \frac{S_f}{d}t \tag{6}$$

where τ_f is the observed carrier decay time constant and p_0 is the carrier concentration after the initial rise following carrier injection at the front surface. The slope of a semilog plot of p vs t should thus yield S_f if the sample thickness (d) is known.

Analysis of the carrier concentration decay data (such as Figure 2d) at various illumination levels using eq 6 yielded $S_f \approx (1.0 \pm 0.4) \times 10^2$ cm s^{-1} ($\tau_f \approx 1.0 \times 10^2$ μs) for the Si/CH_3OH−$Me_2Fc^{+/0}$ contact. This value is in good agreement with the value of $S_f = 40$ cm s^{-1} determined previously for the (111) orientation of Si in this electrolyte using radio-frequency and microwave conductivity decay methods.[15]

The photovoltage rise data can also be evaluated through the use of an analytical, approximate solution to the diffusion equation. Since τ_f is relatively large, the photovoltage rise dynamics can be modeled during the 3 μs signal rise time by assuming negligible recombination over this time period. When

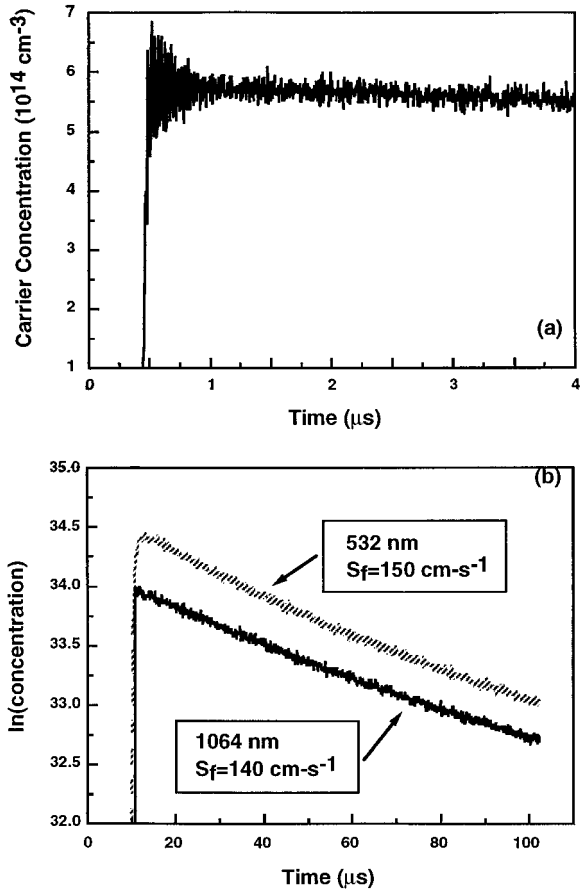

Figure 3. Measurements of the carrier concentration rise (a) and decay (b) (calculated from $V_{p+,oc} - V_{n+,oc}$) at a Si/CH_3OH−1.0 M $LiClO_4$−25 mM Me_2Fc−25 mM Me_2FcBF_4 junction under 1064 nm pulsed laser illumination (≈3 × 10^{-7} J cm^{-2}). For comparison, the decay signal obtained at the same semiconductor/liquid junction under 532 nm illumination at a slightly higher injection level (≈2 × 10^{-6} J cm^{-2}) is also presented (dashed line). The corresponding S_f values were obtained from linear fits to the decay portions of these data (eq 6).

the carrier transport process is dominated by diffusion, carriers generated by an initial illumination pulse at the Si front surface will diffuse toward the back of the semiconductor as given by eq 7:

$$\frac{\partial p(x,t)}{\partial t} = D\frac{\partial^2 p(x,t)}{\partial x^2} \tag{7}$$

Here, $p(x,t)$ represents the photogenerated carrier concentration, and D is the ambipolar diffusion coefficient of electrons and holes in Si ($D = 18$ cm^2 s^{-1}).[12,16−18] A similar equation holds for $n(x,t)$, but since $n(x,t) \approx p(x,t)$ under high level injection conditions, a solution for only one carrier type is required to describe the entire system.

Because the 10 ns laser pulse used in our experiments was much shorter than the time scale of interest (>1 μs), a delta function could be used to approximate the temporal component of the photogeneration process, $G(x,t)$. Thus,

$$G(x,t) = \begin{cases} f(x) & \text{at } t = 0 \\ 0 & \text{at } t > 0 \end{cases} \tag{8}$$

with $f(x)$ representing the distance-dependent carrier profile immediately after the absorption of light, can be used to obtain an approximate solution to eq 7. An analytical solution to eq 7 with an arbitrary function $f(x)$ as the initial condition is readily obtained:[19,20]

$$p(x,t) = \frac{1}{d}\int_0^d f(x')\,dx' + \frac{2}{d}\sum_{i=1}^{\infty}\exp\left(-\frac{i^2\pi^2 Dt}{d^2}\right)\cos\left(\frac{i\pi x}{d}\right)\int_0^d f(x')\cos\left(\frac{i\pi x'}{d}\right)dx' \tag{9}$$

Since the penetration depth of 532 nm light in Si is accurately known, the actual form of $f(x)$ is readily incorporated into eq 9 to obtain the desired approximate solution to eq 7. However, a further simplification was also possible. Because the absorption coefficient of Si for 532 nm illumination is about 8 × 10^3 cm^{-1},[21] almost all of the photogenerated carriers were created within 1 μm of the semiconductor surface. Since the overall sample thickness was ≈100 μm, the initial carrier distribution function ($f(x)$) can be well-approximated as a delta function with respect to distance:

$$f(x) = \begin{cases} I_0' & \text{at } x = 0 \\ 0 & \text{at } x > 0 \end{cases} \tag{10}$$

where $x = 0$ is the semiconductor/liquid interface and I_0' (cm^{-2}) is the total number of carriers generated in the sample by the laser pulse. Using eqs 9 and 10, a simplified expression for the carrier concentration at the back contacts is therefore

$$p(d,t) = \frac{I_0'}{d} + \frac{2I_0'}{d}\sum_{i=1}^{\infty}(-1)^i\exp\left(-\frac{i^2\pi^2 Dt}{d^2}\right) \tag{11}$$

In eq 11, I_0'/d represents the number of photogenerated carriers averaged over the entire semiconductor sample.

This analytical, but approximate, solution was used to fit the carrier concentration rise profiles in Figure 2c. As solution absorption and sample reflectivity precluded an exact measurement of the actual number of photons absorbed by the Si, the value of I_0' was calculated from the maximum carrier concentration reached after 3 μs, $p(d,t>3\ \mu s) \approx p(d,\infty) = I_0'/d$. This is consistent with the assumption of negligible carrier recombination in eqs 7−11. The only adjustable parameter used in the fitting procedure was the sample thickness, d. The value obtained from the fit, $d = 107$ μm, agreed well with the calculated sample thickness of 113 ± 5 μm.[22] The excellent fit of eq 11 to the carrier concentration rise profile (Figure 2c) demonstrated that, under high level injection conditions, diffusion, as opposed to drift, was the predominant carrier transport process in the semiconductor. Furthermore, the quality of the fit justified the assumptions used in eqs 7−11 that recombination occurred at a much slower rate than diffusion and that recombination could be neglected in analyzing the initial carrier concentration rise at the back of the sample.

3. Digital Simulation of Carrier Transport and Decay Dynamics. A more rigorous description of the photovoltage transient signal, including both the rise and decay kinetics, required incorporation of transport and generation as well as recombination processes over the entire experimental time regime. Although the analytical solutions described above yielded an excellent description of the system, further corroboration of the approximations described above required an exact solution of the transport dynamics. In the digital simulation, the complete diffusion, generation, and surface recombination equations were solved over the entire time regime.[10] The bulk recombination process was not included in the simulations due to the very long bulk lifetime of the samples. Input variables such as the ambipolar diffusion coefficient D, the sample thickness d, the photon penetration depth, and the injected carrier density were known independently, so S_f, which dominated the form of the decay (vide supra), was the only

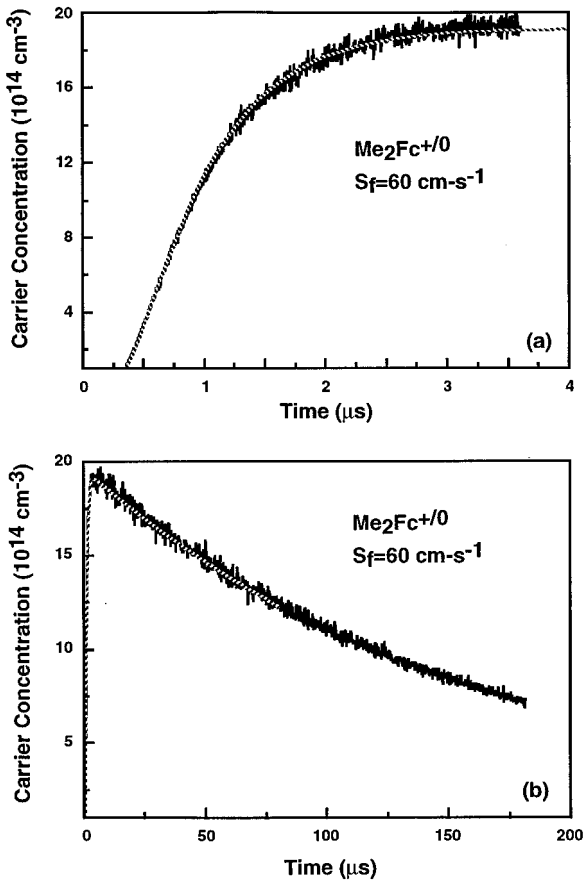

Figure 4. Digital simulation fits (dashed lines) to the carrier rise and decay data calculated from the $V_{p+,oc} - V_{n+,oc}$ measurements presented in Figure 2a,b. The following parameters were used to generate the simulation results: intrinsic carrier concentration of 1.45×10^{10} cm^{-3}, dopant concentration of 3×10^{13} cm^{-3}, injection level of 2.1×10^{13} cm^{-2} (assuming a delta function laser pulse), photon penetration depth of 1.2 μm, ambipolar diffusion coefficient of 18 cm^2 s^{-1}, sample thickness of 107 μm, and the surface recombination velocity of 60 cm s^{-1}.

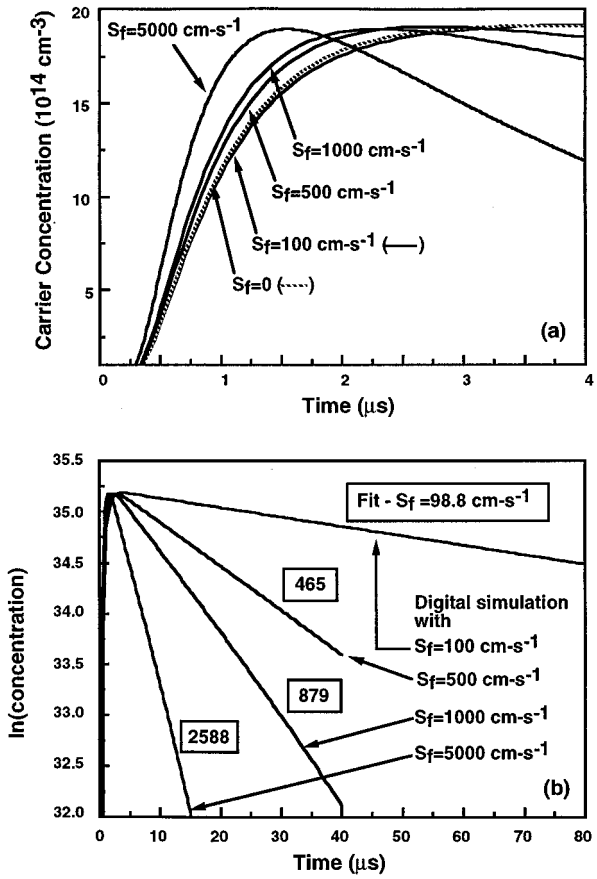

Figure 5. Digital simulation of the carrier concentration rise and decay at various surface recombination velocities. The injection level has been adjusted for various S_f values to the same maximum carrier concentration level: 2.15×10^{13} cm^{-2} for the S_f of 100 cm s^{-1}, 2.47×10^{13} cm^{-2} for the S_f of 500 cm s^{-1}, 2.82×10^{13} and 5.45×10^{13} cm^{-2} for the S_f values of 1000 and 5000 cm s^{-1}, respectively. All other parameters used in the simulation were the same as the ones used in the simulation of Figure 4. The dashed line in (a) was calculated from eq 11, by assuming zero surface recombination. The numbers presented in the rectangular boxes in (b) were S_f values calculated (using eq 6) from the slope of the linear fit to the decay portion of the corresponding curves.

adjustable parameter in the modeling. The light pulse was treated as a delta function with respect to time (eq 8), but the actual value of the optical penetration depth was used in calculating the initial carrier distribution profile. Since the front surface recombination dominated the recombination processes of the entire semiconductor/liquid junction, the back surface recombination velocity was assumed to be zero, so $S(0,t) = S_f$ and $S(d,t) = 0$. For a given value of S_f, the simulation directly yielded the carrier concentration profiles as a function of time.

Figure 4 compares the results of experiment and simulation for the Si/$CH_3OH-Me_2Fc^{+/0}$ contact. The dashed curves in Figure 4a,b indicate that the agreement between theory and experiment for Si/$CH_3OH-Me_2Fc^{+/0}$ contacts with $S_f = 60$ cm s^{-1} is outstanding over the entire time range. The agreement between this S_f value and the S_f obtained from Figure 2d supported the earlier assignment of the concentration decay for the Si/$CH_3OH-Me_2Fc^{+/0}$ contact to the fundamental filament decay mode.

Figure 5 illustrates the effect of varying S_f on the simulated time-dependent carrier concentrations at the back of the sample. For our sample thickness of $\approx$110 μm, the simulated rising portions of the transients were sensitive to changes in S_f for $500 < S_f < 5000$ cm s^{-1}. The data of Figure 5 also allow validation of the approximations used in eqs 7−11, which neglected recombination to describe the photovoltage signal increase for $t \leq 2$ μs. For an interface with an actual value of $S_f = (1.0 \pm 0.4) \times 10^2$ cm s^{-1}, the digital simulation assuming $S_f = 0$ agreed with the experimental photovoltage rise data (Figure 5). The simulation with $S_f = 0$ also agreed, to within the precision of the simulation (<5%) over the carrier concentration rise time (Figure 5a), with the approximate analytical solution that assumed no recombination in this time regime. This agreement further justified the assumption used in the analysis of eqs 7−11 that diffusion occurred on a much faster time scale than front surface recombination at Si/$CH_3OH-Me_2Fc^{+/0}$ contacts.

As the simulated front surface recombination velocity was increased, the signal rise and decay at the back contacts involved a combination of the diffusion and recombination processes. Figure 5b presents a semilog plot of the carrier concentration decays obtained from the digital simulation using S_f values of 100, 500, 1000, and 5000 cm s^{-1}, respectively. This figure also presents comparisons between these simulations and the values of S_f that would be computed from the slope of a linear fit to the concentration decays using the approximate analysis of eqs 5 and 6. For $S_f = 100$ cm s^{-1}, the S_f value calculated using eq 6 differed by less than 2% from the actual S_f value obtained from a best-fit digital simulation of the data. The deviation between the approximate S_f value and the true S_f obtained from the best-fit simulation increased to 10% for $S_f = 1000$ cm s^{-1} and differed by over 40% for $S_f = 5000$ cm s^{-1}. These errors in the S_f values calculated using the analytical expression for carrier decay (eqs 5 and 6) indicated that negligible error occurred when the approximate analytical solutions were used

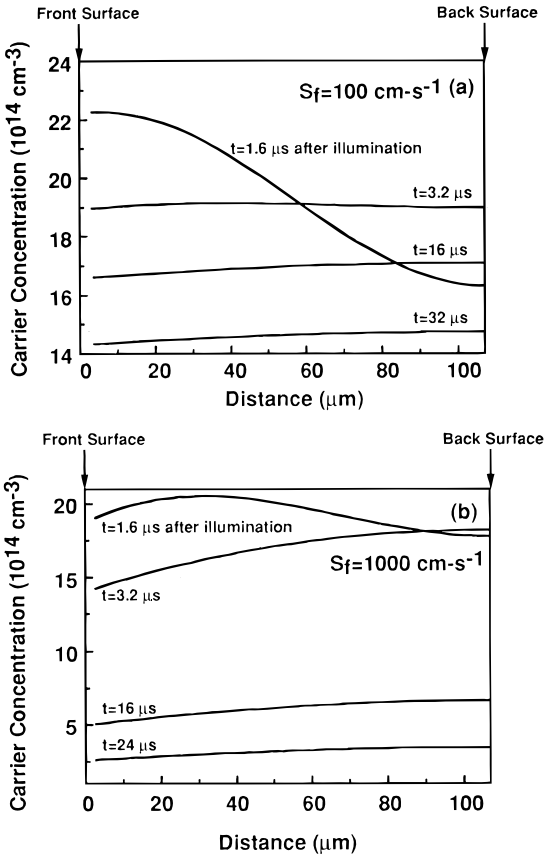

Figure 6. Digital simulation of the carrier concentration vs distance after various time intervals following the illumination at the Si electrode, with a 532 nm pulsed laser. All parameters used in the simulation were the same as those used in Figure 5.

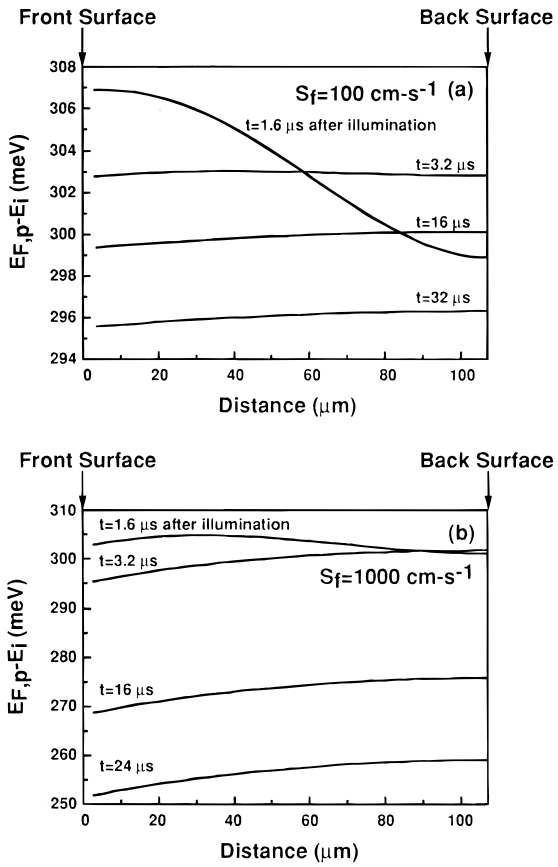

Figure 7. Digital simulation of the quasi-Fermi level distance profile after various time intervals following the illumination at the Si electrode with a 532 nm pulsed laser. All parameters used in the simulation were the same as those used in Figure 5. The quasi-Fermi levels were calculated from the carrier concentrations of Figure 6 using eq 12.

to analyze actual experimental data for the Si/CH_3OH-Me_2-$Fc^{+/0}$ contact.

The digital simulation was also used to model the transport dynamics for the photovoltage signal displayed in Figure 3 after excitation with 1064 nm illumination. Because the absorption coefficient of Si at 1064 nm is only about 10 cm^{-1} at this illumination wavelength,[21] carriers were generated throughout the semiconductor. Under these excitation conditions, the rise time of the concentration profile was much shorter (cf, Figure 3a) and was limited by the laser pulse width. However, the carrier decay time (cf, Figure 3b) and the calculated S_f value were the same as those obtained using 532 nm illumination. These observations experimentally confirmed the assumption used above that carrier recombination occurred on a time scale much longer than that of the initial diffusion process. These experimental results were also predicted by a comparison of the digital simulation for the decays after 532 and 1064 nm excitation in these samples.

4. Time Dependence of Carrier Concentration Profiles and Quasi-Fermi Levels in the Sample. After validation of the photovoltage modeling, the digital simulation was then used to compute the carrier concentration profiles as a function of distance at various times after the initial excitation pulse. Because S_f was determined from fits to the experimental data, there were no adjustable parameters in this aspect of the modeling. Figure 6 depicts the hole concentration profile after several time intervals following the initial excitation pulse, and Figure 7 depicts the corresponding quasi-Fermi level position of holes ($\mathbf{E}_{F,p}$) relative to the intrinsic level ($\mathbf{E}_i$).[5]

$$\mathbf{E}_{F,p}(x,t) - \mathbf{E}_i(x,t) = kT \ln\left[\frac{p(x,t)}{n_i}\right] \qquad (12)$$

For the S_f value of 100 cm s^{-1}, the difference between $\mathbf{E}_{F,p}(d,t)$ and $\mathbf{E}_{F,p}(0,t)$ at $t = 32$ μs after excitation was less than 1 meV. Even for $S_f = 1000$ cm s^{-1}, $\mathbf{E}_{F,p}(d,t) - \mathbf{E}_{F,p}(0,t)$ was less than 10 meV, i.e., $<kT$, 16 μs after the excitation. Thus, the experimentally measured values at the back of the sample yielded excellent approximations to the desired quasi-Fermi levels at the solid/liquid contact. Table 1 presents the difference between $\mathbf{E}_{F,p}(d,t)$ and $\mathbf{E}_{F,p}(0,t)$ obtained from the modeling at various S_f values. These values can be used to correct the experimentally determined $\mathbf{E}_{F,p}(d)$ values to the desired $\mathbf{E}_{F,p}(0)$ values if a precision $\ll kT$ in determination of the surface quasi-Fermi level values is required. Under the high level injection conditions, the electron concentration is the same as the hole concentration, so the gradient in $\mathbf{E}_{F,n}$ can be corrected in an analogous fashion.

B. Time-Resolved Photovoltage Measurements of Si/THF−CH_3OH−$Me_{10}Fc^{+/0}$, Si/CH_3OH−$MV^{2+/+}$, and Si/CH_3OH−$CoCp_2^{+/0}$ Contacts. Transient photovoltage data were also collected for three other redox couples: $Me_{10}Fc^{+/0}$, $MV^{2+/+}$, and $CoCp_2^{+/0}$. Such data are valuable for several reasons: (a) they validated the transport model described above for other solid/liquid contacts, (b) they allowed a quantitative evaluation of the surface recombination velocity for Si/CH_3-OH junctions in the presence of various other redox couples, and (c) they provided values for the gradients of the quasi-Fermi levels to ensure that the steady-state values of $\mathbf{E}_{F,n}(d)$ and $\mathbf{E}_{F,p}(d)$ measured experimentally provided valid estimates of the desired $\mathbf{E}_{F,n}(0)$ and $\mathbf{E}_{F,p}(0)$ energies at the semiconductor/liquid interfaces.

The transient photovoltage decays (converted into carrier concentration decays) for Si/THF-CH_3OH−$Me_{10}Fc^{+/0}$ and Si/

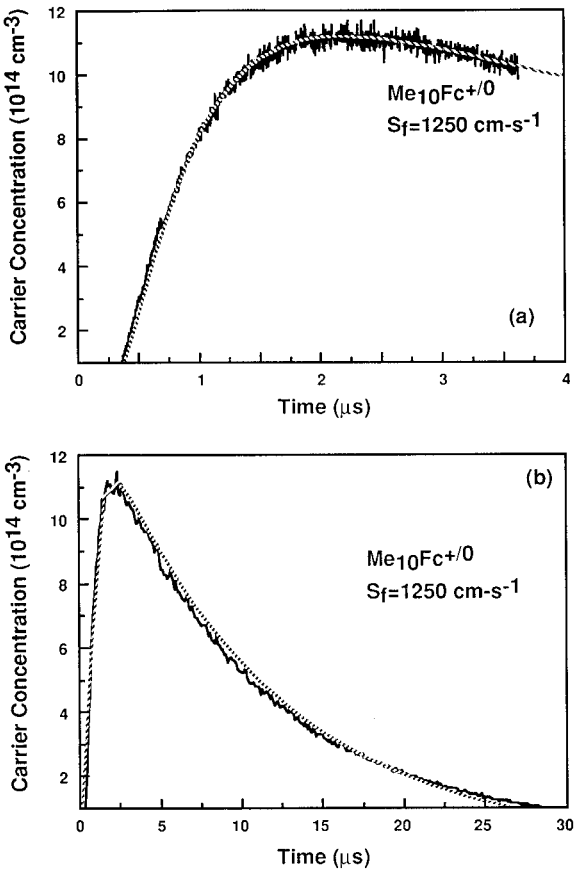

Figure 8. Measurements (solid lines) and simulation fits (dashed lines) of the carrier concentration rise and decay (calculated from $V_{p+,oc} - V_{n+,oc}$) at a Si/80% THF−20% CH_3OH (v/v)−0.55 M $LiClO_4$−23 mM $Me_{10}Fc$−14 mM $Me_{10}FcBF_4$ junction under 532 nm pulsed laser illumination (≈3×10^{-5} J). The injection level used in the simulation was 1.76×10^{13} cm^{-2}, and the value of the surface recombination velocity was 1250 cm s^{-1}. All other parameters were the same as those in Figure 4.

TABLE 1: Digital Simulation of the Quasi-Fermi Level Differences (in meV) between the Back of the Semiconductor Sample and the Semiconductor/Liquid Interface ($\mathbf{E}_{F,p}(d,t) - \mathbf{E}_{F,p}(0,t)$) at Various S_f Values[a]

	t,[b] μs			
S_f, cm/s	1.6	3.2	16	32
100	−8.0[c]	<0.1	0.8	0.7
500	−5.2[c]	2.9	3.6	3.7
1000	−1.8[c]	6.3	7.1	7.6
5000	19.4	26.5	33.5	

[a] The values of the parameters used in the simulation were the same as those used in Figure 5. [b] All data were obtained at the end of the time interval (t) during the simulation process. [c] The negative value implied that $\mathbf{E}_{F,p}(0,t)$ at the semiconductor/liquid interface was more positive than the hole quasi-Fermi level at the back surface, $\mathbf{E}_{F,p}(0,t) > \mathbf{E}_{F,p}(d,t)$.

$CH_3OH-MV^{2+/+}$ contacts are shown in Figures 8 and 9. The digital simulations of these data are also included in the figures. The value of S_f was 1000 ± 300 cm s^{-1} for the Si/THF−CH_3-OH-$Me_{10}Fc^{+/0}$ junction at various light intensities, and was 800 ± 200 cm s^{-1} in the $CH_3OH-MV^{2+/+}$ solutions. These S_f values are in accord with the lower V_{oc} values, and the larger inferred surface recombination velocities, that were observed in steady-state $J-V$ measurements of Si/liquid contacts in these electrolytes (part 1[6]) as compared to the high V_{oc} and low S_f value (≈100 cm s^{-1}) displayed by the Si/$CH_3OH-Me_2Fc^{+/0}$ system. These S_f values are also in accord with expectations based on the Shockley−Read−Hall recombination theory, as discussed further in section IV.

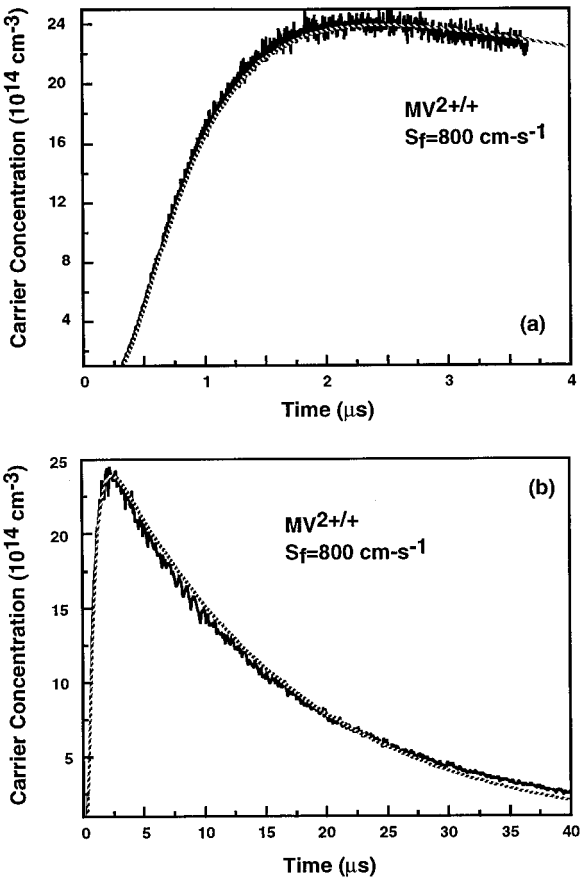

Figure 9. Measurements (solid lines) and simulation fits (dashed lines) of the carrier concentration rise and decay (calculated from $V_{p+,oc} - V_{n+,oc}$) at a Si/CH_3OH−1.1 M LiCl−16 mM MV^+−23 mM $MVCl_2$ junction under 532 nm pulsed laser illumination (≈7×10^{-4} J incident onto the cell). The injection level used in the simulation was 3.38×10^{13} cm^{-2}, and the value of the surface recombination velocity was 800 cm s^{-1}. All other parameters were the same as those in Figure 4.

Even with these higher S_f values, measurement of $\mathbf{E}_{F,p}$ (or $\mathbf{E}_{F,n}$) at $x = d$ (i.e., at the back surface of the Si sample) yielded little error in $\mathbf{E}_{F,p}(0)$ (or $\mathbf{E}_{F,n}(0)$) after very short time periods. Reference to Table 1 shows that for $S_f = 1000$ cm s^{-1} the potential difference was only 7.6 mV across the semiconductor 32 μs after the illumination pulse. These results suggested that the quasi-Fermi levels of carriers were essentially flat in the Si samples used in our experiments and, consequently, that the quasi-Fermi levels measured at the back contacts were accurate descriptions of the quasi-Fermi positions at the semiconductor/liquid interfaces.

The only anomalous decay dynamics were those of Si/CH_3-OH−$CoCp_2^{+/0}$ contacts. The photovoltage decay data, converted into carrier concentrations (Figure 10), consisted of two primary components. A best fit yielded $S_f = 750$ cm s^{-1} for $t < 10$ μs, and $S_f = 275$ cm s^{-1} for $t > 20$ μs. The origin of the fast component in the decays remains unclear at this time. The slower surface recombination rate observed at longer times is consistent with the overall high V_{oc} values exhibited by these contacts.[6]

C. Modeling of the Steady-State Carrier Concentration vs Distance Profiles for Si/CH_3OH Liquid Contacts. In addition to the real-time photovoltage data and modeling described above, it was also of interest to analyze the steady-state photovoltage data for the various Si/CH_3OH contacts. A validated treatment of the transport dynamics in the steady-state situation would allow evaluation of the quasi-Fermi level gradients without reference to any of the transient data. A critical test of the entire model would therefore be provided by

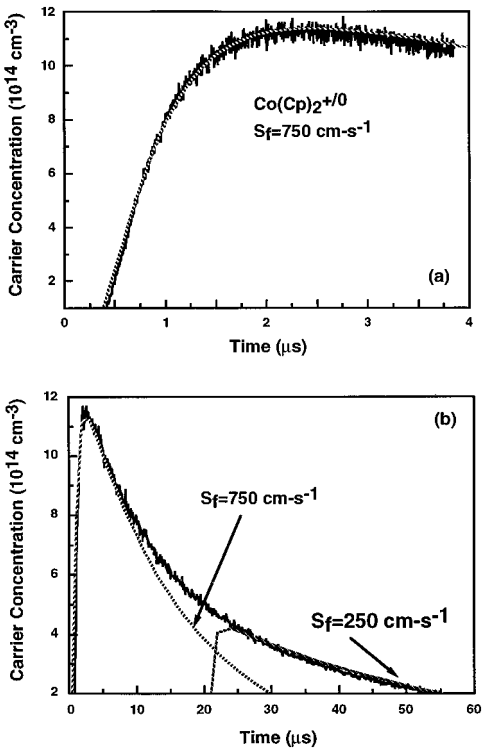

Figure 10. Measurements (solid lines) and simulation fits (dashed lines) of the carrier concentration rise and decay (calculated from $V_{p+,oc} - V_{n+,oc}$) at a Si/CH_3OH−1.0 M LiCl−8.5 ± 0.5 mM $CoCp_2$−38 mM $CoCp_2Cl$ junction under 532 nm pulsed laser illumination. The injection level used in the simulation was 1.56×10^{13} cm^{-2}, and the value of the surface recombination velocity was 750 cm s^{-1}. In (b), the slower decay component at longer time was also fitted with the digital simulation, using an S_f value of 250 cm s^{-1}.

the agreement (or lack thereof) between these two independent methods for determining S_f and $\mathbf{E}_{F,p}(d,t) - \mathbf{E}_{F,p}(0,t)$.

The steady-state condition was readily analyzed because of the small thickness and large carrier lifetime of our sample, which allowed simplification of the relevant differential equations. For relatively low surface recombination velocities, the electron and hole concentrations will be approximately constant throughout the specimen. Under the steady-state open-circuit conditions, the generation rate equals the recombination rate. Thus, from eq 4, we have

$$I_0 - I_0 \exp(-\alpha d) = pS_f = n_i \exp\left(\frac{qV_{p+,oc} - qV_{n+,oc}}{2kT}\right)S_f \quad (13)$$

where p, the hole concentration, is assumed to be independent of both time and distance. I_0 is the flux of photons absorbed at the semiconductor front surface (photons cm^{-2} s^{-1}), and α is the absorption coefficient (cm^{-1}) of Si at a particular wavelength of illumination. The charge carrier generation rate can be estimated from the limiting photocurrent density, $J_{ph}/q = I_0 - I_0 \exp(-\alpha d)$, assuming a quantum yield of unity for collection of photogenerated carriers. Therefore, a specific, experimentally measured, quasi-Fermi level separation, $q(V_{p+,oc} - V_{n+,oc}) = \mathbf{E}_{F,p}(d) - \mathbf{E}_{F,n}(d)$, corresponds to a unique value of S_f. This provides a simple method for ensuring that $|\mathbf{E}_{F,p}(d) - \mathbf{E}_{F,p}(0)| \ll kT$ and $|\mathbf{E}_{F,n}(d) - \mathbf{E}_{F,n}(0)| \ll kT$.

As reported in part 1,[6] the steady-state open-circuit potential at the n^+ points of Si/CH_3OH−$Me_2Fc^{+/0}$ contacts was −550 ± 30 mV vs the solution potential (at a light-limited photocurrent density $J_{ph} = 3.5$ mA cm^{-2}). In addition, the value of $V_{p+,oc}$ at this light intensity was ≈0 mV. The value of S_f calculated from $V_{p+,oc} - V_{n+,oc}$ using eq 13 was 45 ± 25 cm s^{-1}, which is similar to the S_f obtained from the transient studies.

A more rigorous analytical solution was also pursued in order to evaluate quantitatively the values of $\mathbf{E}_{F,n}(d,t) - \mathbf{E}_{F,n}(0,t)$ and $\mathbf{E}_{F,p}(d,t) - \mathbf{E}_{F,p}(0,t)$. At steady state, the carrier concentrations $n(x)$ and $p(x)$ are given by the standard relationship between transport, diffusion, recombination, and generation:[23]

$$D\frac{d^2p(x)}{dx^2} - \frac{p(x)}{\tau_b} + I_0\alpha \exp(-\alpha x) = 0 \quad (14)$$

where $p(x)$ is the hole concentration at distance x and τ_b is the bulk carrier lifetime at x. Under high level injection conditions, $n(x) \approx p(x)$, so only a solution for one type of carrier is required, although an equation analogous to eqs 13 could also be used to calculate the electron concentration.

Because the $V_{p+,oc} - V_{n+,oc}$ values for identical Si samples that contained highly passivated front contacts to minimize the surface recombination process in air were larger than any of the $V_{p+,oc} - V_{n+,oc}$ values observed for the Si/CH_3OH contacts studied herein, recombination at the semiconductor/liquid junction could be identified as the dominant carrier recombination process. The back surface recombination velocity was therefore neglected in the steady-state analysis. The following boundary conditions were imposed on the solution to eq 14:

$$-D\left.\frac{dp(x)}{dx}\right|_{x=d} = 0 \quad (15)$$

$$-D\left.\frac{dp(x)}{dx}\right|_{x=0} = p(0)S_f \quad (16)$$

Equation 14 was simplified by assuming that the bulk recombination rate, τ_b, was independent of distance. Therefore, the solution for $p(x)$ is

$$p(x) = C_0 \exp(-\alpha x) + C_1 \exp\left(\frac{x}{L}\right) + C_2 \exp\left(-\frac{x}{L}\right) \quad (17)$$

with

$$C_0 = \frac{I_0\alpha}{1/\tau_b - D\alpha^2} \quad (18)$$

$$C_1 = \frac{\alpha \exp(-\alpha d) - \dfrac{\alpha + S_f/D}{1/L + S_f/D}\dfrac{\exp(-d/L)}{L}}{\dfrac{\exp(d/L)}{L} - \dfrac{\exp(-d/L)}{L}\dfrac{1/L - S_f/D}{1/L + S_f/D}} C_0 \quad (19)$$

$$C_2 = \frac{1/L - S_f/D}{1/L + S_f/D} C_1 - \frac{\alpha + S_f/D}{1/L + S_f/D} C_0 \quad (20)$$

In these equations, L is the diffusion length of holes, so $L = (D\tau_b)^{1/2}$.

Using eq 4, $p(d)$ could be calculated from the value of $V_{p+,oc} - V_{n+,oc}$ that was measured under steady-state, high level injection conditions. Since I_0, D, d, and α were known, and $\tau_b \approx 1$ ms,[12] eqs 17−20 could be solved for the unique value of S_f that was required to produce the measured values of $V_{p+,oc} - V_{n+,oc}$. This modeling thus directly yielded values for the carrier concentration profiles as a function of distance throughout the sample. From eq 12, the distance profile of the hole quasi-Fermi level, $\mathbf{E}_{F,p}(x)$, could then be calculated. This calculation provided a quantitative value for the difference between the quasi-Fermi level positions at the back and front of the sample for each carrier type.

Table 2 displays the values of S_f that were obtained from this steady-state, high level injection modeling procedure. As

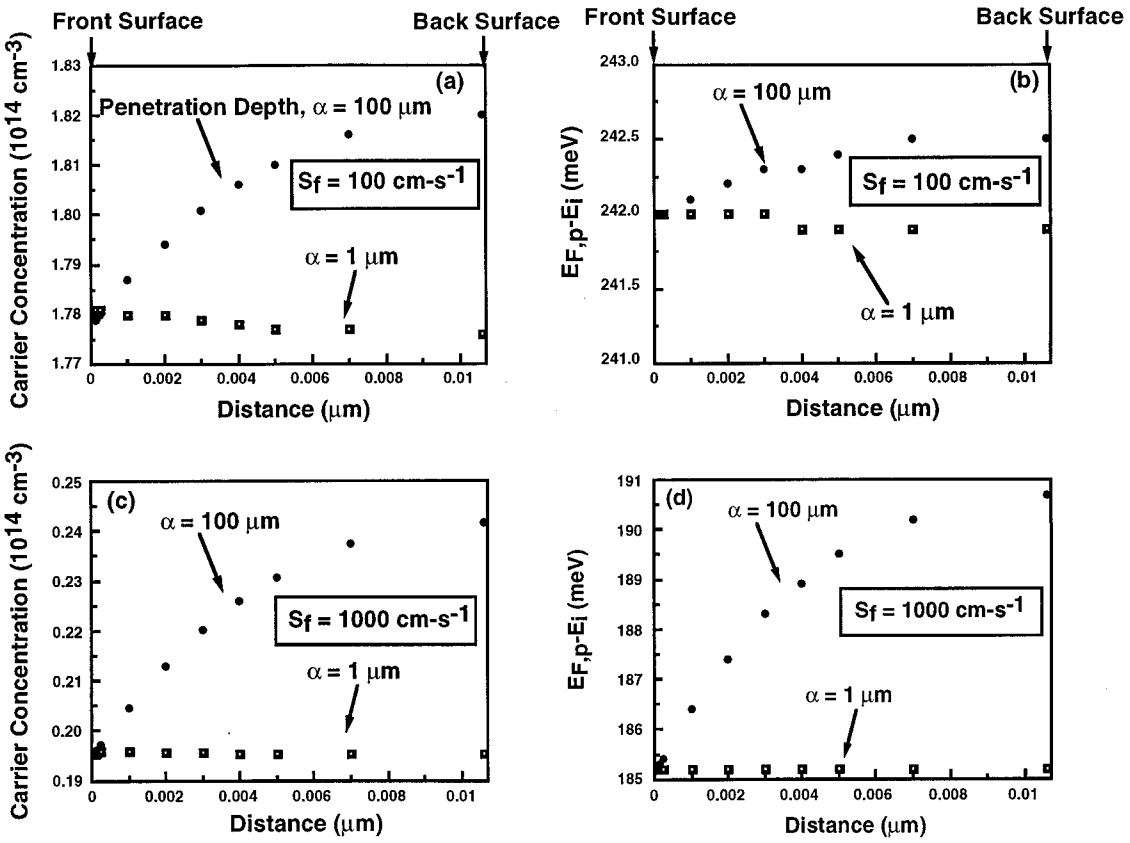

Figure 11. Steady-state carrier concentration and quasi-Fermi level profiles under illumination with a photon penetration depth of 1 or 100 μm.

TABLE 2: Steady-State Calculation of the Front Surface Recombination Velocity, S_f, for Si Samples in Contact with Various Redox Couples

	$Me_2Fc^{+/0}$ [a]	$Me_{10}Fc^{+/0}$ [b]	$MV^{2+/+}$ [c]	$CoCp_2^{+/0}$ [d]
$V_{p+,oc} - V_{n+,oc}$ (mV)[e]	517	419	391	485
J_{ph} (mA cm^{-2})	3.15	3.99	2.30	3.39
S_f (cm s^{-1})[f]	5×10^1	8×10^2	9×10^2	1.2×10^2
$\mathbf{E}_{F,p}(d) - \mathbf{E}_{F,p}(0)$ (meV)[g]	−0.1	<0.1	<0.1	−0.1
$\mathbf{E}_{F,p}(d) - \mathbf{E}_{F,p}(0)$ (meV)[h]	0.3	4.5	4.9	0.7

[a] Obtained in CH_3OH−1.0 M $LiClO_4$−11 mM Me_2Fc−16 mM Me_2FcBF_4. [b] Obtained in 80% THF−20% CH_3OH (v/v)−0.54 M $LiClO_4$−23 mM $Me_{10}Fc$−14 mM $Me_{10}FcBF_4$. [c] Obtained in CH_3OH−1.1 M LiCl−17 mM MV^+−23 mM $MVCl_2$. [d] Obtained in CH_3OH−0.90 M LiCl−2.3 ± 0.2 mM $CoCp_2$−45 mM $CoCp_2Cl$. [e] The differences in open-circuit potentials measured at the p^+ and n^+ contact points, $V_{p+,oc} - V_{n+,oc}$, at the short-circuit current density levels reported in the table. [f] The surface recombination velocity calculated using eqs 17−20. The number of photons absorbed by the semiconductor, I_0, was obtained from the J_{ph} values assuming 100% internal carrier collection efficiency at short circuit, $I_0 = J_{ph}/(q(1 - \exp(-\alpha d)))$, where d is the thickness of the sample, $d = 107$ μm in this simulation. [g] The difference in the quasi-Fermi level of holes between the back surface and the front surface at a photon penetration depth of 1 μm ($\alpha = 1 \times 10^4$ cm^{-1}). [h] Same as *g*, but at a photon penetration depth of 100 μm ($\alpha = 1 \times 10^2$ cm^{-1}).

expected, contacts with the largest V_{oc} values produced the smallest surface recombination velocities. The S_f values were, in general, in excellent agreement with the values determined from the transient photovoltage decay measurements (vide supra), lending further support to the hypothesis that charge carrier motion was predominantly driven by diffusion in these high injection samples.

For Si/CH_3OH−$Me_2Fc^{+/0}$ and Si/CH_3OH−$CoCp_2^{+/0}$ contacts, which displayed the highest $V_{p+,oc} - V_{n+,oc}$ values and therefore had the lowest surface recombination velocities, the maximum error in $|\mathbf{E}_{F,p}(d) - \mathbf{E}_{F,p}(0)|$ (and in $|\mathbf{E}_{F,n}(d) - \mathbf{E}_{F,n}(0)|$) was <2 meV (i.e., $\ll kT$) for a photon penetration depth of 100 μm. This small gradient in the quasi-Fermi level energy was a consequence of the relatively thin samples, combined with the high carrier diffusion coefficient, long bulk carrier lifetime (>1 ms), and small surface recombination velocities (<200 cm s^{-1}) that were characteristic of the Si/CH_3OH−$Me_2Fc^{+/0}$ and Si/CH_3OH−$CoCp_2^{+/0}$ contacts studied in this work. For Si/CH_3OH−$MV^{2+/+}$ and Si/THF−CH_3OH-$Me_{10}Fc^{+/0}$ contacts, S_f was somewhat larger. However, even for these contacts, the maximum difference in the quasi-Fermi level positions between the back and front of the sample was 5 meV. This simulation thus showed that the experimentally measured $\mathbf{E}_{F,n}$ and $\mathbf{E}_{F,p}$ values were close approximations to the values at the front surface. In addition, the simulation provided an analytical means for precisely correcting the experimentally determined values to obtain $\mathbf{E}_{F,p}(0,t)$ and $\mathbf{E}_{F,n}(0,t)$ for all the systems of interest (Table 2).

This steady-state carrier modeling was also useful in predicting the behavior of $V_{p+,oc} - V_{n+,oc}$ as a function of the illumination wavelength. Figure 11 shows the carrier concentration profiles and quasi-Fermi level positions that were calculated for high- and low-energy monochromatic illumination (1 and 100 μm penetration depths), respectively. For a fixed S_f value at constant illumination, $\mathbf{E}_{F,p}(d)$ was not a strong function of wavelength. The largest calculated change in $\mathbf{E}_{F,p}(d)$ when the penetration depth was varied from 1 to 100 μm was <6 meV (for $S_f = 1000$ cm s^{-1}).

This prediction was verified experimentally for Si/CH_3OH−$Me_2Fc^{+/0}$ and Si/THF−CH_3OH−$Me_{10}Fc^{+/0}$ contacts, for which $V_{p+,oc} - V_{n+,oc}$ was measured as a function of wavelength (at a constant carrier injection level). The values for $V_{p+,oc} - V_{n+,oc}$ (Table 3) were independent of wavelength within the error of the measurements (±5 mV). Thus, the $\mathbf{E}_{F,n}$ and $\mathbf{E}_{F,p}$ values determined under polychromatic illumination were representative of the quasi-Fermi level positions for this specific injection level at the various Si/CH_3OH redox couple interfaces.

TABLE 3: $V_{p+,oc} - V_{n+,oc}$ Values as a Function of Wavelength for a Si Electrode in Contact with a CH_3OH−1.0 M $LiClO_4$−58 mM Me_2Fc−2.0 mM Me_2FcBF_4 Solution or a 80% THF−20% CH_3OH (v/v)−0.54 M $LiClO_4$−24 mM $Me_{10}Fc$−17 mM $Me_{10}FcBF_4$ Solution

	λ, nm							
	457	514	760	820	880	940	980	1020
$Me_{10}Fc^{+/0}$ [a]	336		337	338		336	333	
$Me_{10}Fc^{+/0}$ [b]		374			377	376	373	376
$Me_2Fc^{+/0}$ [c]	539	537			540		536	540

[a] Measured at $J_{sc} = 0.21$ mA cm^{-2}. [b] Measured at $J_{sc} = 0.81$ mA cm^{-2}. [c] Measured at $J_{sc} = 1.7$ mA cm^{-2}.

IV. Discussion

The results presented above clearly indicate that a diffusional model of charge carrier separation and movement satisfactorily describes the real-time and steady-state photovoltage properties of Si/CH_3OH contacts under high level injection conditions. This behavior fully supports the analysis of the steady-state $J-V$ properties presented in parts 1 and 2[6,7] and validates the approximation that the quasi-Fermi levels determined at the back of these samples were good approximations to the values near the solid/liquid contact.

In this work, photovoltage rise and decay data were exploited to investigate the charge carrier dynamics. For conventional photoelectrodes under low level injection conditions, the photovoltage exhibits an extremely rapid rise time which is usually limited by the bandwidth of the measuring instrumentation. This limitation occurs because the photovoltage under low level injection is produced predominantly by charge separation across the depletion region, driven by drift, which occurs in <1 ps.[8,9] In the absence of a significant interfacial electric field to separate charge, however, diffusion processes are required for effective charge movement. This mode of transport should result in a relatively slow rise time of the photovoltage, with a functional form predictable by standard diffusional models. The time scales of the measurements of the transient photovoltage rise, as well as the functional form of these signals, clearly indicated the validity of these predictions for the studies discussed above.

The experimental and theoretical description of this photoelectrode system has also allowed rigorous estimation of the gradient in quasi-Fermi levels from the back to the front of the sample. In most cases, errors of $\ll kT$, and as small as <1 meV, result from the use of values at the back of the sample. Note that by assuming all of the recombination occurred at the front surface of the sample, these gradients are larger than the ones that would be computed assuming that some of the carrier recombination proceeded in the bulk of the sample and/or at the back contacts. This assumption of front surface-dominated recombination was justified in all but possibly one case. For Si/CH_3OH−$Me_2Fc^{+/0}$ contacts, the measured S_f value (100 ± 40 cm s^{-1}) was very similar to the S_f value (50 ± 10 cm s^{-1}) measured for the sample in air, for which the front surface of the sample was passivated to minimize front surface recombination. Thus, a rigorous correction can be made for the quasi-Fermi level gradients in all systems studied, except for the CH_3OH−$Me_2Fc^{+/0}$ contact. In the Si/CH_3OH−$Me_2Fc^{+/0}$ system, where S_f is so small that recombination at the back contact may contribute to the total observed recombination dynamics, a rigorous estimate of the quasi-Fermi level gradients indicates that these gradients are less than 1 meV (Tables 1 and 2). The gradients may possibly be smaller than this limiting value, depending on the precise value of the surface recombination velocity at the back of the sample.

The data and modeling also have yielded values for the recombination rates at the semiconductor/liquid contact as a function of the electrochemical potential of the redox couple, $\mathbf{E}(A/A^-)$. The values of S_f were observed to be smaller in solutions having electrochemical potentials near the conduction band edge, $\mathbf{E}_c$, or the valence band edge, $\mathbf{E}_v$, of the semiconductor than in solutions having $\mathbf{E}(A/A^-)$ in the middle of the semiconductor band gap. These recombination data are in agreement with the predictions of the Shockley−Read−Hall model for recombination, which suggests that recombination is more favored when the equilibrium Fermi level position is near the middle of the semiconductor band gap.[14] To our knowledge, the observations described herein are the first experimental validation of this prediction for semiconductor surfaces in contact with outer-sphere redox couples.

Another striking feature of the photovoltage decay analysis is the relatively small surface recombination velocities that have been obtained for all the redox couples investigated in this study. These relatively low values have been obtained even though significant concentrations of both forms of the redox reagent were present in solution and could therefore act simultaneously as electron and hole trapping sites. These low surface recombination velocities underscore the rather slow interfacial charge transfer dynamics of photogenerated charge carriers with these outer-sphere redox couples, regardless of the energetics for charge carrier capture at the Si/CH_3OH interface. Such low surface recombination rates are essential for high photoelectrochemical efficiencies under high level injection conditions, because otherwise the photogenerated carriers would be consumed unproductively through recombination at the solid/liquid interface. For example, using eqs 4 and 17−20, a value for S_f of 10^7 cm s^{-1} would only produce a V_{oc} of 270 mV at $J_{ph} = 3.5$ mA cm^{-2}, which is much lower than the V_{oc} values determined in part 1 for Si/CH_3OH contacts[6] and would not even allow the sample to be in high level injection at this illumination intensity.[24] The low S_f values measured herein also are essential in preventing significant gradients of the quasi-Fermi levels in the sample (Figure 7 and Tables 1 and 2), so that measurements at the back of the specimen yield the desired information on the carrier concentrations at the solid/liquid contact. Our data indicate that low S_f behavior appears to be a general property of the Si/CH_3OH interface in contact with outer-sphere redox couples and is not specifically confined to the Si/CH_3OH−$Me_2Fc^{+/0}$ system, for which low charge-transfer velocities were previously documented.[15] The maximum surface recombination velocity measured for the solutions studied herein was <1500 cm s^{-1}; this corresponds to an upper limit for the interfacial charge-transfer rate constant of 10^{-16} cm^4 s^{-1} (assuming a 10 mM electron donor or acceptor concentration) for the rate-determining interfacial charge-transfer process; otherwise, the measured carrier recombination velocity at the solid/liquid junction would be larger than that observed experimentally. This upper limit on the interfacial charge-transfer rate constant agrees with recent theoretical predictions for charge transfer at semiconductor/liquid junctions[25] and with independent measurements of the interfacial charge-transfer rate constant for well-defined semiconductor surfaces in contact with outer-sphere redox couples.[26,27]

The rather low surface recombination velocities are also required for, and are fully consistent with, the high photoelectrochemical energy conversion efficiencies that have been reported previously for n-Si and for nearly intrinsically doped Si/CH_3OH−$Me_2Fc^{+/0}$ contacts.[28−30] These low surface recombination velocities, which correspond to approximately one electrical defect for every 100 000 surface atoms,[31] underscore the high degree of electrical perfection that is achievable through the use of well-controlled semiconductor/liquid contacts.

V. Conclusions

We have demonstrated that the quasi-Fermi levels of electrons and holes can be measured directly, and that little error arises from measurement of these values at the back of well-designed, selectively contacted, Si samples. Analysis of the real-time photovoltage rise and decay measurements using analytical models and digital simulation methods has confirmed that, under high level injection conditions, carrier transport in these Si specimens is predominantly driven by diffusion. Modeling of the steady-state open-circuit condition has yielded surface recombination velocities that are in agreement with those obtained from an analysis of the transient photovoltage signals. The highest recombination velocity of the contacts studied was less than 1500 cm s^{-1}, whereas the lowest value of S_f was ≈100 cm s^{-1}. The surface recombination velocities were larger for solutions with electrochemical potentials near the middle of the semiconductor bandgap than for solutions with electrochemical potentials close to the conduction or valence band edges. The low surface recombination velocities also agreed with theoretical and experimental estimates of interfacial charge-transfer rate constants for semiconductor/liquid contacts. These measurements have established that efficient photoelectrochemical energy conversion can be achieved through use of diffusionally driven concentration gradients and that the quasi-Fermi level concept has validity under our experimental conditions.

The data presented here, combined with those described in parts 1 and 2,[6,7] comprise a relatively complete picture of the recombination processes that occur at the Si/CH_3OH contact. With such electrically passive surfaces, efficient charge separation can be effected through either drift or diffusionally driven processes. These types of samples are extremely interesting from a fundamental viewpoint, because they have allowed measurement of the theoretically important quasi-Fermi levels and also have allowed a detailed analysis of the spatial and temporal gradients of the carrier concentrations in the samples under a variety of conditions. These samples also should provide insight into the transport and recombination processes that are characteristic of semiconductor particles, which generally are sufficiently small that diffusionally driven concentration gradients, as opposed to drift, dominate the charge separation dynamics.

Acknowledgment. We gratefully acknowledge the National Science Foundation, Grant CHE-9634152, for support of this work. M.X.T. is grateful to the Link Energy Foundation and to the W.R. Grace foundation for graduate fellowships, and O.K. gratefully acknowledges the Deutsche Forschungsgemeinschaft for a postdoctoral fellowship. We are grateful to Drs. R. Sinton and R. Swanson of Sunpower, Inc., for helpful discussion and for supplying the samples used in this work.

References and Notes

(1) Gerischer, H. In *Physical Chemistry: An Advanced Treatise*; Eyring; H., Henderson, D., Yost, W., Eds.; Academic: New York, 1970; Vol. 9A, p 463.

(2) Fonash, S. J. *Solar Cell Device Physics*; Academic: New York, 1981.

(3) Reineke, R.; Memming, R. *J. Phys. Chem.* **1992**, *96*, 1317.

(4) Laibinis, P. E.; Stanton, C. E.; Lewis, N. S. *J. Phys. Chem.* **1994**, *98*, 8765.

(5) Sze, S. M. *The Physics of Semiconductor Devices;* 2nd ed.; John Wiley and Sons: New York, 1981.

(6) Tan, M. X.; Kenyon, C. N.; Krüger, O.; Lewis, N. S. *J. Phys. Chem.* **1997**, *101*, 2830.

(7) Krüger, O.; Kenyon, C. N.; Tan, M. X.; Lewis, N. S. *J. Phys. Chem.* **1997**, *101*, 2840.

(8) Willig, F. *Ber. Bunsen-Ges. Phys. Chem.* **1988**, *92*, 1312.

(9) Willig, F.; Bitterling, K.; Charlé, K.-P.; Decker, F. *Ber. Bunsen-Ges. Phys. Chem.* **1984**, *88*, 374.

(10) Ryba, G. N. Ph.D. Thesis, California Institute of Technology, 1992.

(11) *Modular Series on Solid State Devices*; 2nd ed.; Neudeck, G. W.; Pierret, R., Eds.; Addison-Wesley: Reading, MA, 1989; Vol. II.

(12) Swanson, R. M. *Solar Cells* **1986**, *17*, 85.

(13) Shockley, W. *Electrons and Holes in Semiconductors*; Van Nostrand: New York, 1950.

(14) Many, A.; Goldstein, Y.; Grover, N. B. *Semiconductor Surfaces*; North-Holland : New York, 1965; p 496.

(15) Forbes, M. D. E.; Lewis, N. S. *J. Am. Chem. Soc.* **1990**, *112*, 3682.

(16) Carrier−carrier scattering increases as a function of carrier concentration and reduces the mobility and therefore the diffusion coefficients of electrons and holes. In our simulation, such variations could be neglected to within 5% for carrier concentrations between 5×10^{13} and 10^{16} cm^{-3}.

(17) Thurber, W. R.; Mattis, R. L.; Liu, Y. M.; Filliben, J. J. *J. Electrochem. Soc.* **1980**, *127*, 2291.

(18) Thurber, W. R.; Mattis, R. L.; Liu, Y. M.; Filliben, J. J. *J. Electrochem. Soc.* **1980**, *127*, 1807.

(19) Carslaw, H. S.; Jaeger, J. C. *Conduction of Heat in Solids;* 2nd. ed.; Oxford University Press: Oxford, 1959.

(20) The symbol x' represents the distance term used in the integration between 0 and d.

(21) Aspnes, D. E. In *Properties of Silicon*; INSPEC: London, 1988.

(22) This measured thickness resulted from the etchant-induced removal of 7 μm from the originally 120 ± 5 μm thick sample; see part 1 (ref 6) for a detailed description of the etching process.

(23) Blakemore, J. S. *Semiconductor Statistics*; Dover: New York, 1987; p 381.

(24) An acceptor concentration of 10 mM and an electron-transfer rate constant of 10^{-12} cm^4 s^{-1}, as has been proposed previously for p-InP photoelectrodes (Rosenwaks, Y.; et al. *J. Phys. Chem.* **1994**, *98*, 2739), yields $S = 10^7$ cm s^{-1}. Such large S_f values would not only be inconsistent with the measured S_f values of this study but would preclude the operation of these samples in high level injection conditions at our light intensities and would be incompatible with the photoelectrochemical behavior reported in parts 1 and 2 of this work.

(25) Lewis, N. S. *Annu. Rev. Phys. Chem.* **1991**, *42*, 543.

(26) Pomykal, K. E.; Fajardo, A. M.; Lewis, N. S. *J. Phys. Chem.* **1996**, *100*, 3652.

(27) Fajardo, A. M.; Lewis, N. S. *Science* **1996**, *274*, 969.

(28) Kumar, A.; Lewis, N. S. *Appl. Phys. Lett.* **1990**, *57*, 2730.

(29) Gibbons, J. F.; Cogan, G. W.; Gronet, C. M.; Lewis, N. S. *Appl. Phys. Lett.* **1984**, *45*, 1095.

(30) Tan, M. X.; Kenyon, C. N.; Wilisch, W. C. A.; Lewis, N. S. *J. Electrochem. Soc.* **1995**, *142*, L62.

(31) The surface recombination velocity is given by the relation $S = N_s v_{th} \sigma$. A rough estimate yields a surface state density of $N_s = 10^{10}$ cm^{-2} using a surface recombination velocity $S = 100$ cm s^{-1}, a thermal velocity of the carriers of $v_{th}=10^7$ cm s^{-1}, and a capture cross section of $\sigma = 10^{-15}$ cm^2.